Atmos. Chem. Phys., 22, 4339–4353, 2022
https://doi.org/10.5194/acp-22-4339-2022

Atmospheric Chemistry and Physics
Open Access
EGU

Seasonal characteristics of atmospheric peroxyacetyl nitrate (PAN) in a coastal city of Southeast China: Explanatory factors and photochemical effects

Taotao Liu[1,2,3], Gaojie Chen[1,2,3], Jinsheng Chen[1,2], Lingling Xu[1,2], Mengren Li[1,2], Youwei Hong[1,2], Yanting Chen[1,2], Xiaoting Ji[1,2,3], Chen Yang[1,2,3], Yuping Chen[1,2,3], Weiguo Huang[4], Quanjia Huang[5], and Hong Wang[6]

[1]Center for Excellence in Regional Atmospheric Environment, Institute of Urban Environment, Chinese Academy of Sciences, Xiamen, China
[2]Key Lab of Urban Environment and Health, Institute of Urban Environment, Chinese Academy of Sciences, Xiamen, China
[3]University of Chinese Academy of Sciences, Beijing, China
[4]State Key Laboratory of Structural Chemistry, Fujian Institute of Research on the Structure of Matter, Chinese Academy of Sciences, Fuzhou, China
[5]Xiamen Environmental Monitoring Station, Xiamen, China
[6]Fujian Meteorological Science Institute, Fujian Key Laboratory of Severe Weather, Fuzhou, China

Correspondence: Jinsheng Chen (jschen@iue.ac.cn) and Youwei Hong (ywhong@iue.ac.cn)

Received: 13 November 2021 – Discussion started: 21 December 2021
Revised: 6 March 2022 – Accepted: 8 March 2022 – Published: 5 April 2022

Abstract. Peroxyacetyl nitrate (PAN) acting as a typical indicator of photochemical pollution can redistribute NO_x and modulate O_3 production. Coupled with the observation-based model (OBM) and a generalized additive model (GAM), the intensive observation campaigns were conducted to reveal the pollution characteristics of PAN and its impact on O_3, the contributions of influencing factors to PAN formation were also quantified in this paper. The F values of GAM results reflecting the importance of the influencing factors showed that ultraviolet radiation (UV; F value = 60.64), O_x ($O_x = NO_2 + O_3$, 57.65), and air temperature (T, 17.55) were the main contributors in the PAN pollution in spring, while the significant effects of O_x (58.45), total VOCs (TVOCs, 21.63), and T (20.46) were found in autumn. The PAN formation rate in autumn was 1.58 times higher than that in spring, relating to the intense photochemical reaction and meteorological conditions. Model simulations revealed that acetaldehyde oxidation (46 % ± 4 %) contributed to the dominant formation pathway of PA (hence PAN), followed by methylglyoxal oxidation (28 % ± 3 %) and radical cycling (19 % ± 3 %). The PAN formation was highly VOC sensitive, as surplus NO_x (compared with VOCs abundance) prevented NO_x from being the limiting factor photochemical formation of secondary pollution. At our site, PAN promoted and inhibited O_3 formation under high and low RO_x levels, respectively. The PAN promoting O_3 formation mainly occurred during the periods of 11:00–16:00 (local time) when the favourable meteorological conditions (high UV and T) stimulated the photochemical reactions to offer RO_x radicals, which accounted for 17 % of the whole monitoring periods in spring and 31 % in autumn. The analysis of PAN formation mechanism and its positive or negative effect on ozone provided scientific insights into photochemical pollution mechanisms under various pollution scenarios in coastal areas.

1 Introduction

Peroxyacetyl nitrate ($CH_3C(O)O_2NO_2$, PAN) is a key product of photochemical smog (Penkett and Brice, 1986; Li et al., 2019). PAN is generated through photochemical reactions of precursors emitted by human activities only, and the atmospheric PAN is a reliable and scientific indicator of photochemical pollution (Lonneman et al., 1976; Han et al., 2017). In the surface atmosphere, the level of PAN is much lower than that of ozone (O_3), but its biological toxicity is about one or two magnitudes greater than that of O_3 (Temple and Taylor, 1983). Additionally, PAN acts as a temporary reservoir for NO_x and radicals, and can transport to remote regions to redistribute NO_x and intervene in O_3 production at regional or even global scale (Kleindienst, 1994; Atkinson et al., 2006; Fischer et al., 2010).

The reaction of peroxyacetyl radical ($CH_3C(O)O_2$, PA) with NO_2 is the only formation pathway of PAN (Han et al., 2017; Xue et al., 2014). PAN affects radical chemistry and modulates O_3 production mainly by affecting PA radical, which is one of the most abundant organic peroxy radicals in the troposphere (Tyndall et al., 2001). Only a small group of oxygenated volatile organic compounds (OVOCs), i.e. acetaldehyde (CH_3CHO), methacrolein (MACR), methyl vinyl ketone (MVK), methyl ethyl ketone (MEK), and methylglyoxal (MGLY), can directly produce PA radical to generate PAN (Xue et al., 2014; Zhang et al., 2015). A large proportion of these OVOCs (the second-generation precursors of PAN) are mainly transformed by oxidation reactions from some hydrocarbons such as ethane, propene, isoprene, and aromatics (the first-generation precursors of PAN; Xu et al., 2021; Qian et al., 2019). The main and direct PAN destruction is thermal decomposition, and the indirect sinks of PAN were the reactions of PA with NO, HO_2, and RO_2 (Wolfe et al., 2014; Zeng et al., 2019).

Some studies on the distribution and sources of PAN have been conducted in urban, suburban, and remote regions around the world (Grosjean et al., 2002; Marley et al., 2007; Roberts et al., 2001). The PAN levels in cities are higher than those in rural and remote areas, and those in background areas such as oceans and mountains can be as low as tens of parts per trillion by volume (pptv; Gaffney et al., 1999; Moore and Remedios, 2010). Despite the growing concerns about photochemical pollution in China, PAN measurements and analysis of its photochemical mechanism are still sparse (Zeng et al., 2019). At present, the observations of PAN were mainly distributed in Beijing, Guangzhou, and Hong Kong (Xue et al., 2014; Yuan et al., 2018; Zeng et al., 2019). Xue et al. (2014) reported that anthropogenic VOCs were the most important precursors of PAN in urban areas, and isoprene was the predominant precursor in suburban regions. In the study by Zeng et al. (2019), carbonyls were the most significant contributors to PAN production, followed by aromatics and BVOCs. In addition, some researchers found that atmospheric PAN suppressed local O_3 formation in autumn (Zeng et al., 2019). Recently, negative and positive impacts of PAN photochemistry on O_3 production were captured under the low and high NO_x conditions, respectively (Zeng et al., 2019; Liu et al., 2021). However, the PAN formation and its influencing mechanism on O_3 production are still complex and unclear (Hu et al., 2020; Zhang et al., 2019; Xu et al., 2018). Long-term field measurements and model simulations could help to verify the mechanisms under various pollution scenarios and environmental conditions.

Xiamen is located in the coastal region of Southeast China under the East Asian monsoon control, belonging to the subtropical marine climate (Liu et al., 2020a, b). In spring, north cold airflow and south warm airflow formed the quasi-stationary front causing atmospheric stagnation. In autumn, under the control of the West Pacific subtropical high (WPSH), favourable meteorological conditions enhanced the formation and accumulation of photochemical pollutants (Wu et al., 2020). Our previous studies focused on the occurrence and pollution characteristics of PAN (Hu et al., 2020). In this study, an observation-based model coupled to the Master Chemical Mechanism (OBM-MCM) was used to better understand PAN photochemistry in spring and autumn, and a generalized additive model (GAM) was adopted to quantify the complex non-linear relationships of PAN with its precursors and environmental factors (Hua et al., 2021). The study aims to explore (1) the PAN formation mechanism and sensitivity analysis, (2) the impacts of PAN on O_3 formation and radical chemistry, and (3) the relationship between PAN and influencing factors under different pollution scenarios.

2 Materials and methods

2.1 Observation site

Observations were carried out at the Atmospheric Environment Observation Supersite (AEOS, 24.61° N, 118.06° E; Fig. 1), located on the rooftop of an approximately 70 m high building in the Institute of Urban Environment, Chinese Academy of Sciences. The observation site is surrounded by highways, educational institutions, and residential buildings, all of which characterize rapid urbanization development. When the prevailing wind direction was southerly, our observation site was downwind of the densely populated downtown (i.e. Xiamen Island; Hu et al., 2020; Liu et al., 2022). The field observations were continuously conducted from 15 March to 4 November 2020. The photochemical pollution events mainly appeared during spring and autumn in Xiamen, and we preferred to choose the periods with relatively high O_3 and PAN levels, then the measured data of 53 d in each season was chosen after excluding some special circumstances, such as extreme synoptic situations and instrument calibration.

2.2 Measurement techniques

PAN was monitored using a PAN analyser (PANs-1000, Focused Photonics Inc., Hangzhou, China) containing gas chromatography with electron capture detector (GC-ECD). During the observation period, multi-point standard curve calibration was conducted once a month, and single-point calibration was conducted every week, respectively. In the calibration mode of the PAN analyser, the mass flow controller (MFC) controls the flow rate of NO, acetone, and zero gas separately. The PAN standard gas is generated by the reaction of NO and acetone under ultraviolet light irradiation, and the sample is diluted to the required calibration mixing ratio for injection analysis. PAN was detected every 5 min and the detection limit was 50 pptv. The uncertainty and precision of PAN measurement were ±10 % and 3 %, respectively.

A gas chromatography mass spectrometer (GC-FID/MS, TH-300B, Wuhan, China) was used for monitoring the atmospheric VOCs with a 1 h time resolution. The instrument conducted sampling with a 30 L min^{-1} sampling rate, then samples were pre-concentrated by cooling to −160 °C in a cryogenic trap followed by heating to 100 °C, and subsequently transferred to the secondary trap by high-purity helium (He). The flame ionization detector (FID) detected the low-carbon (C_2-C_5) hydrocarbons by a PLOT (Al_2O_3/KCl) column (15 m × 0.32 mm × 6.0 µm); the other species were quantified using a DB-624 column (60 m × 0.25 mm × 1.4 µm). The instrument system can quantitatively analyse 106 VOCs in the ambient atmosphere, including 29 alkanes, 11 alkenes, 1 alkyne, 17 aromatics, 35 halogenated hydrocarbons, and 13 OVOCs. Nine compounds (acetaldehyde, propanal, crotonaldehyde, methacrolein, n-butanal, benzaldehyde, valeraldehyde, m-tolualdehyde, and hexanal) could not be determined due to lack of aldehyde and ketone calibration gases, and Table S2 in the Supplement shows all VOC compounds that we used in the OBM model. The single-point calibration was performed every day at 23:00 local time with the standard mixtures of PAMS and TO15, and multi-point calibration was performed for 1 month. The detection limits of the measured VOCs were in the range of 0.02–0.30 parts per billion by volume (ppbv), and the measurement precision was ≤ 10 %.

Criteria air pollutants of O_3, CO, SO_2, and NO_x were monitored by using Thermo Instruments TEI 49i, 48i, 43i, and 42i (Thermo Fisher Scientific, Waltham, MA, USA), respectively. HONO was monitored using an analyser for Monitoring Aerosols and Gases in Ambient Air (MARGA, ADI 2080, Applikon Analytical B.V., the Netherlands). Particulate matters ($PM_{2.5}$) were monitored by oscillating microbalance with tapered element (TEOM1405, Thermo Scientific Corp., MA, USA). The meteorological parameters (i.e. wind speed (WS), wind direction (WD), pressure (P), air temperature (T), and relative humidity (RH)) were measured by a weather station with sonic anemometer (150WX, Airmar, Milford, NH, USA). Ultraviolet radiation (UV) was determined by a UV radiometer (KIPP & ZONEN, SUV5 Smart UV Radiometer). Photolysis frequencies including $J(O^1D)$, $J(NO_2)$, $J(HONO)$, $J(NO_3)$, $J(HCHO)$, and $J(H_2O_2)$ were analysed by a photolysis spectrometer (PFS-100, Focused Photonics Inc., Hangzhou, China), and the uncertainty and detection limit of photolysis rate measurement were ±5 % and around 1×10^{-5}, respectively.

Table S1 in the Supplement shows the detailed uncertainty and detection limit of instruments for trace gas observation. A schedule was applied to operate and inspect the AEOS monitoring station regularly and strictly to ensure the validity of the data. The detailed applications of the atmospheric monitoring procedure were shown in our previous studies (Wu et al., 2020; Liu et al., 2020a, b; Hu et al., 2020).

2.3 Observation-based model

The OBM-MCM model is successfully used in the simulation of photochemical processes and the quantification of the reaction rates, such as O_3, PAN, and alkyl nitrates ($RONO_2$; Zeng et al., 2019). In our study, the PAN photochemistry mechanism was simulated using this box model, and the incorporated chemical mechanism was the latest version of MCM-v3.3.1 (http://mcm.leeds.ac.uk/MCM/, last access: 19 October 2021), which introduced 142 non-methane VOCs and about 20 000 elementary reactions (Jenkin et al., 2003; Saunders et al., 2003). The physical process including dilution effect and dry deposition within the boundary layer height was considered, avoiding the excessive accumulation of pollutants in the model (Li et al., 2018; Liu et al., 2021; Xue et al., 2016). The observed data with a time resolution of 1 h of pollutants (i.e. O_3, CO, NO, NO_2, HONO, SO_2, and VOCs), meteorological parameters (i.e. T, P, and RH), and photolysis rate constants ($J(O^1D)$, $J(NO_2)$, $J(H_2O_2)$, $J(HONO)$, $J(HCHO)$, and $J(NO_3)$), which were mentioned in Sect. 2.1, were input into the OBM-MCM model as constraints. The photolysis rates of other molecules were driven by the solar zenith angle and were scaled by measured JNO_2 (Saunders et al., 2003). Pre-ran for 2 d before running the model helped to constrain the unmeasured compounds reaching a steady state (Xue et al., 2014; Liu et al., 2022).

PAN affects atmospheric photochemistry by acting as a temporary source or sinks of PA radical (Xue et al., 2014; Liu et al., 2021); hence, the production and sink of PA radical reflecting the PAN formation were discussed in our study. Furthermore, relative incremental reactivity (RIR) was used to analyse the sensitivity of O_3 (Eq. 1) and PAN (Eq. 2) to their precursors, and was calculated as the ratio of the differences in O_3 or PAN net production rate to variety in precursors (Chen et al., 2020; Liu et al., 2021). The production pathways of O_3 include $HO_2 + NO$ and $RO_2 + NO$ reactions, and the destruction pathways of O_3 involve reactions of O_3 photolysis, $O_3 + OH$, $O_3 + HO_2$, $O_3 + VOCs$, $NO_2 + OH$, and $NO_3 + VOCs$. The net O_3 production rate ($P(O_3)$) is calculated by the difference of O_3 production rate and destruction

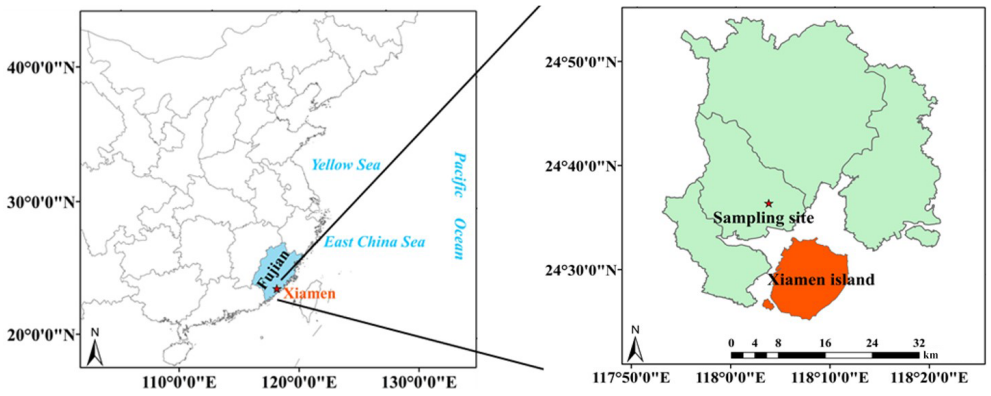

Figure 1. Location of Xiamen and the observation site.

Table 1. Estimated degree (during promotion effect scenarios in spring and autumn) of freedom (Edf), degree of 530 reference (Ref. df), P value, F value, deviance explained (%), adjusted R^2, deviance contribution (%) for the 531 smoothed variables (including NO, Δ RO_x, TVOCs, $PM_{2.5}$, UV, T, RH, and WS) in the multiple-factor GAM model.

	Spring				Autumn			
Smoothed variables	Edf	Ref.df	F value	P value	Edf	Ref.df	F value	P value
NO (ppbv)	5.21	6.26	8.73	0.00	1.11	1.21	4.16	0.03
O_x (ppbv)	4.73	5.85	57.65	0.00	4.84	5.98	58.45	0.00
TVOCs (ppbv)	7.14	8.19	9.52	0.00	4.08	5.06	21.63	0.00
$PM_{2.5}$ ($\mu g\,m^{-3}$)	5.73	6.86	9.94	0.00	1.53	1.90	14.53	0.00
UV ($W\,m^{-2}$)	1.00	1.00	60.64	0.00	4.38	5.38	7.13	0.00
T (°)	1.00	1.00	17.55	0.00	2.73	3.46	20.46	0.00
RH (%)	6.78	7.87	3.40	0.00	6.56	7.68	10.99	0.00
WS ($m\,s^{-1}$)	5.22	6.37	7.42	0.00	5.12	6.28	2.55	0.02
	Deviance explained (%) = 80 %; Adjust $R^2 = 0.79$				Deviance explained (%) = 72 %; Adjust $R^2 = 0.70$			

rate, and the detailed net production rate of O_3 ($P(O_3)$) was introduced in our previous study (Liu et al., 2022). The net production of PAN (P(PAN)) involved the production pathway of PA + NO_2, and the loss of PAN was thermal decomposition and PAN + OH (Zeng et al., 2019):

$$\mathrm{RIR}(O_3) = \frac{\Delta P(O_3)/P(O_3)}{\Delta X/X}, \quad (1)$$

$$\mathrm{RIR}(\mathrm{PAN}) = \frac{\Delta P(\mathrm{PAN})/P(\mathrm{PAN})}{\Delta X/X}, \quad (2)$$

where $\Delta X/X$ represents the reduction in the input mixing ratios of each target O_3, and the PAN precursor group was 20 % (Liu et al., 2021).

2.4 Generalized additive model

The generalized additive model (GAM) is an extension of the additive model proposed. Different from traditional regression models, GAM is a non-parametric regression model driven by data rather than statistical distribution models (He et al., 2017). The GAM does not need to set the parameter model in advance, and it can adjust the functional form of the explained variable according to the specific situation. The GAM has been widely used in air pollution research, such as for O_3 and $PM_{2.5}$, and can effectively deal with the complex non-linear relationship between air pollutants and influencing factors (Ma et al., 2020; Hua et al., 2021; Guan et al., 2019). It is the first time that the GAM has been used to analyse the relationship between PAN and its influencing factors, and the combined effect of multiple influencing factors on the PAN mixing ratio was discussed in our study. Its form is:

$$g(y) = \beta + f_1(x_1) + f_2(x_2) + \ldots + f_n(x_n) + \alpha, \quad (3)$$

where y is the response variable; $g(y)$ is the connection function; x_1, x_2, and x_n are the explanatory variables; $f_1(x_1)$, $f_2(x_2)$, and $f_n(x_n)$ are the non-parametric smoothing functions; and β is the intercept; and α is the truncation error.

The F value, P value, adjust R^2, and deviance explained given by the GAM model are used to judge the significance of the influencing factors on PAN and the accuracy of the

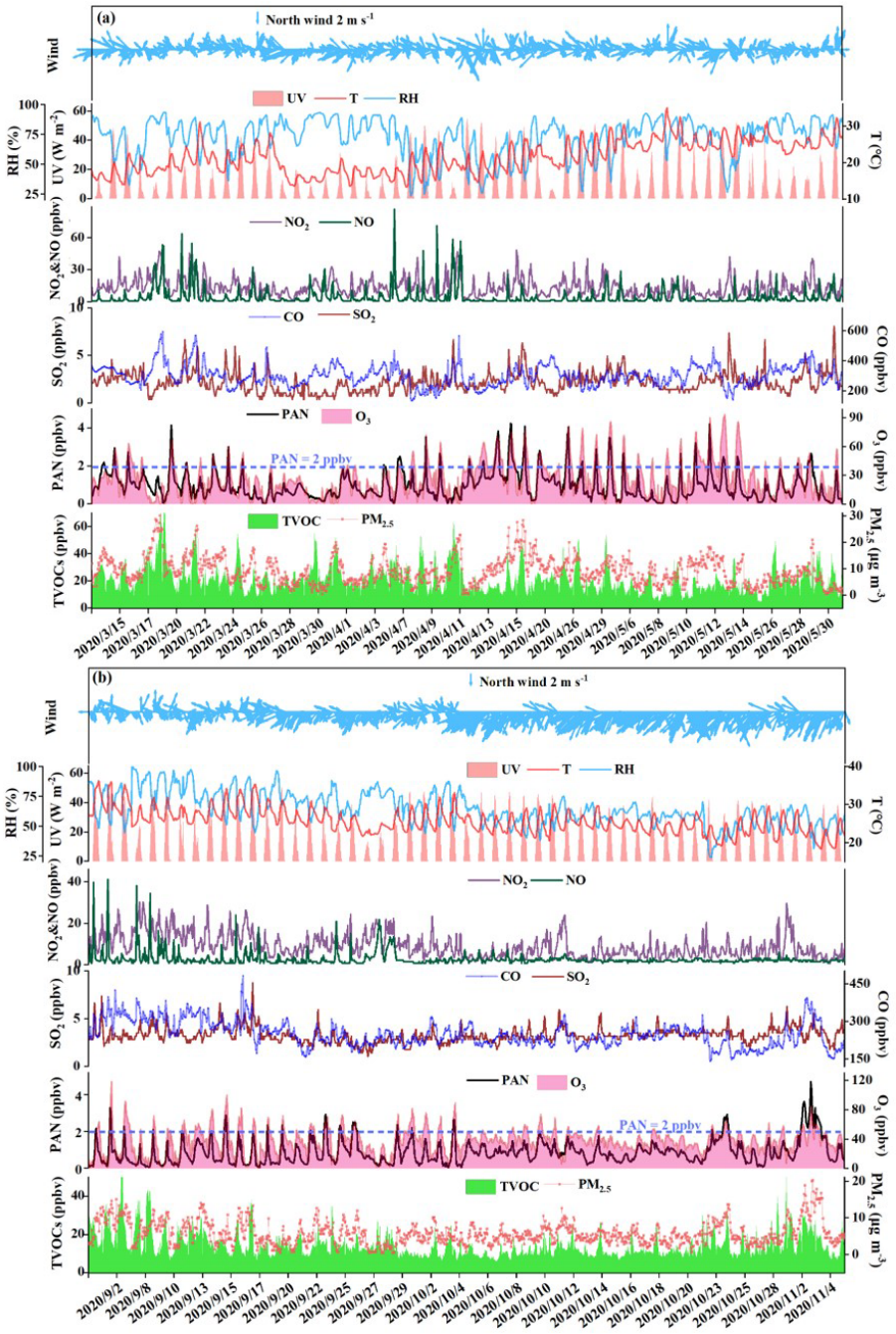

Figure 2. Time series of PAN, O_3, NO_x, CO, SO_2, TVOCs, $PM_{2.5}$, and meteorological parameters in **(a)** spring and **(b)** autumn.

model simulation. Among them, a high F value indicates the great importance of the influencing factor, the P value is used to judge the significance of the model result, the adjusted R^2 is the value of the regression square ranging from 0 to 1, and the deviance explained represents the fitting effect. In addition, when the degree of freedom (edf, ref.df) of the explanatory variable is 1, it indicates that the explanatory variable and the response variable are linear. When the degree is > 1, it is a non-linear relationship.

3 Results and discussion

3.1 Overview of observation

The time series of air pollutants and meteorological parameters are shown in Fig. 2. The average levels of PAN in autumn (0.87 ± 0.66 ppbv) were comparable to those in spring (0.96 ± 0.73 ppbv), while O_3 mixing ratios in autumn (37.22 ± 16.89 ppbv) were 1.39 times higher than those in

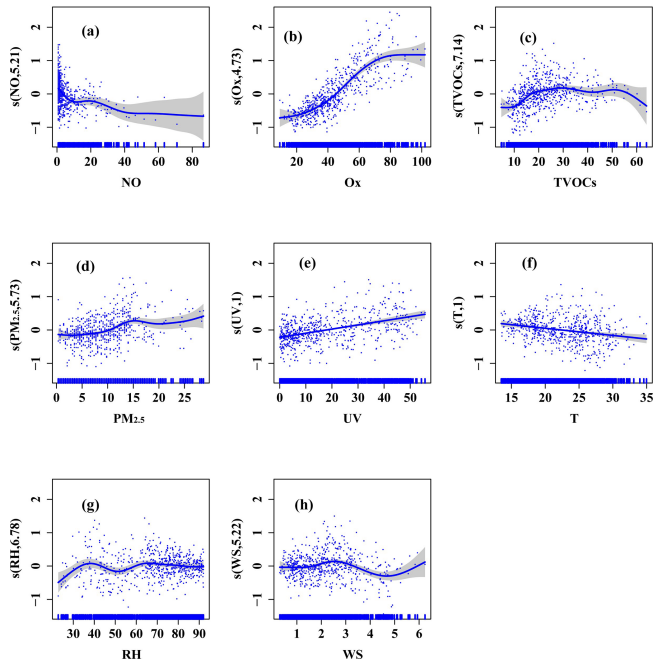

Figure 3. Response curves (spring) in the multiple-factor model of PAN to changes in **(a)** NO, **(b)** O_x ($O_x = O_3 + NO_2$), **(c)** TVOCs, **(d)** $PM_{2.5}$, **(e)** ultraviolet radiation (UV), **(f)** air temperature (T), **(g)** relative humidity (RH), and **(h)** wind speed (WS). The y axis is the smoothing function values. For example, s(NO, df) shows the trend in PAN when NO changes, and the number of df is the degree of freedom. The x axis is the influencing factor, and the shaded area around the solid blue line indicates the 95 % confidence interval of PAN. The vertical short blue lines represent the concentration distribution characteristics of the explanatory variables (units: NO (ppbv), O_x (O_3+NO_2; ppbv), TVOCs (ppbv), $PM_{2.5}$ (μg m^{-3}), UV (W m^{-2}), T (°), RH (%), WS (m s^{-1})).

spring (26.73±18.63 ppbv). PAN and O_3 are produced by the photochemical reactions of VOCs and NO_x; thus, they usually show a relatively close relationship ($R^2 \geq 0.49$, Fig. S3). The PAN level (0.92 ± 0.69 ppbv) in Xiamen was lower than that of megacities such as Beijing (3.79±3.26 ppbv; Xu et al., 2021), Jinan (2.54 ppbv; Liu et al., 2018), Santiago (6.4 ppbv; Rubio et al., 2005), and Chongqing (2.05 ppbv; Sun et al., 2020), and was comparable to the coastal cities with relatively clean air, including Shenzhen (1.01 ± 0.94 ppbv; Xia et al., 2021) and Qingdao (0.81 ppbv; Liu et al., 2021).

The averaged values of PAN and NO, NO_2, CO, and TVOCs in spring were 1.70, 1.32, 1.21, and 1.46 times higher, respectively, than those in autumn. The details of measured VOCs are provided in Table S2 in the Supplement. Alkanes, OVOCs, aromatics, and halocarbons accounted for about 90 % of total VOCs, suggesting the impacts of atmospheric oxidation capacity and marine emissions in coastal regions (Liu et al., 2020a, b). During the transition from spring to summer the wind direction fluctuated between northwest and southeast, while during the transition from summer to autumn the wind direction fluctuated from southeast to northeast. The wind rose charts showed that the wind direction frequencies with relatively high wind speed (> 3 m s^{-1}) in spring and autumn were southeast wind and northeast wind (Fig. S4 in the Supplement), respectively. Although the frequency of northwest wind (NNW) also accounted for a certain proportion, the NNW speeds were generally slow, and the direction of the NNW was mainly rural residential and mountainous areas with less anthropogenic emissions, so it was not the focus of this research. The ultraviolet radiation (UV), WS, and T in spring (15.32 W m^{-2}; 1.96 m s^{-1}; 21.51°) were weaker than those in autumn (18.43 W m^{-2}; 3.01 m s^{-1}; 25.85°), and RH and P in spring (73.25 %; 1010.71 hPa) were higher than those in autumn (65.21 %; 1008.71 hPa). These meteorological conditions carried by the WPSH (high T, low RH, and stagnant weather conditions) were conducive to the photochemical reaction and accumulation of air pollutants in autumn (Wu et al., 2019; Xia et al., 2021). High precursor levels of PAN in spring were conducive to the continuous and stable production of PAN, and the high air temperature in autumn accelerated the thermal decomposition of PAN. However, the O_3 levels in autumn were higher than those in spring, attributing to the influence of strong photochemical reaction conditions, regional transport from the Yangtze River Delta region, or increased atmospheric background levels (Monks, 2000). High O_3 values in both seasons were concentrated on the wind direction of southeast and northeast (Fig. S5 in the Supplement). High PAN values in spring easily happened in the wind direction of the southeast with low wind speed (< 3 m s^{-1}), showing the influence of urban plumes from the downtown of Xiamen Island. High PAN values in autumn also appeared in the wind direction of the southeast, as well as the northeast with a relatively high wind speed (from Quangzhou city, an industrial city adjacent to Xiamen). Moreover, PAN lifetimes in our observation site were relatively short due to the high ambient temperature, and the PAN lifetimes in autumn (2.02 h) were significantly lower than those in spring (6.39 h), which was not conducive to regional transport (Hu et al., 2020; Liu et al., 2018). Accordingly, O_3 showed obvious characteristics of long-range transport, and PAN pollution was mainly from local production and/or accumulation in spring and autumn, but short-range transport from adjacent cities might contribute to the high PAN concentrations in autumn to a certain extent.

Based on the above analysis, we found that the photochemical reactions were still intense and even stronger under the low precursor mixing ratios. Although the precursor mixing ratios of PAN and O_3 in spring were significantly higher than those in autumn ($P < 0.01$), the PAN mixing ratios in autumn were comparable to those in spring, while the O_3 mixing ratios in autumn were much higher than those in spring. Therefore, it is very necessary to further explore the key influencing factors and their formation mechanisms.

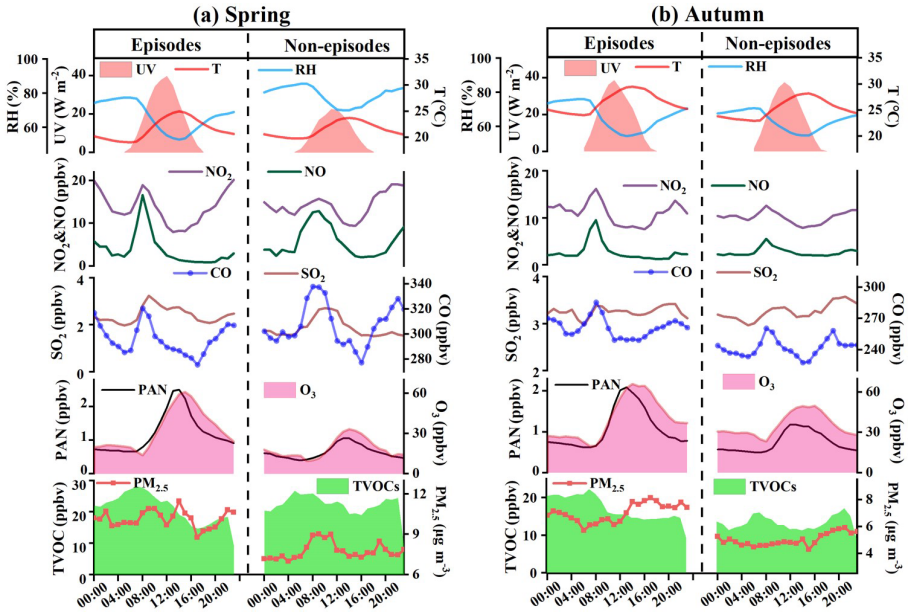

Figure 4. Diurnal trends of PAN, O_3, TVOCs, $PM_{2.5}$, other trace gases, and meteorological parameters during episodes and non-episodes in **(a)** spring and **(b)** autumn, respectively.

3.2 The influencing factors of PAN using the GAM

PAN levels are not only related to chemical reactions in the boundary layer, but also affected by meteorological conditions (Hu et al., 2020). According to the collinearity analysis (He and Lin, 2017), the meteorological parameters (UV, T, RH, and WS) and other air pollutants (NO, TVOCs, $PM_{2.5}$, and O_x) were considered into the multiple-factor GAM model (Table S3 in the Supplement). As shown in Table 1, the adjusted R^2 and deviance explained for the smoothed variables of the multiple-factor GAM model were 0.70 % and 72 % in spring, 0.60 % and 63 % in autumn. According to the F values, the orders of the explanatory variables in spring and autumn were UV (60.64) > O_x (57.65) > T (17.55) > $PM_{2.5}$ (9.94) > TVOCs (9.52) > NO (8.73) > WS (7.42) > RH (3.4) and O_x (58.45) > TVOCs (21.63) > T (20.46) > $PM_{2.5}$ (14.53) > RH (10.99) > UV (7.13) > NO (4.16) > WS (2.55), respectively.

Response curves of the PAN to explanatory factors in the multiple-factor model were presented (Fig. 3 and Fig. S6 in the Supplement). Except for UV and T in spring, the degrees of freedom (df) of the explanatory variables were greater than 1, indicating the non-linear relationships between explanatory variables and PAN. The PAN in both seasons showed a downward trend with the increase of NO. PAN in spring was constant with NO fluctuation between 10 and 23 ppbv, and the confidence interval (CI) of NO concentration was relatively narrow. As we all know, the reaction of PA + NO is one of the most important loss pathways of PA, and the NO_2 production by NO oxidation in the O_3 formation cycle can react with PA radical to produce PAN, suggesting that NO can consume and produce PAN indirectly (Liu et al., 2021). The consumption of NO to PAN was basically equal to the production when the NO levels were relatively high (> 10 ppbv), and the consumption of NO to PAN was greater than the production when the NO levels were low in spring. High values of NO mainly happened during rush hour traffic; thus, controlling vehicle emissions can effectively alleviate PAN pollution. O_x had a positive correlation with PAN, representing the promotion effects of atmospheric oxidation capacity on PAN formation. The O_x levels < 70 ppbv (with narrow CI) played a significant promotion role in PAN formation (Fig. 3b and Fig. S4b in the Supplement). High O_x > 70 ppbv showed little influence on PAN, which could be explained as high O_x with relatively high air temperature leading to intense PAN thermal decomposition. When TVOCs were between 10 and 30 ppbv and $PM_{2.5}$ levels were < 17 μg m^{-3}, PAN showed an upward trend with narrow CI. According to our previous study (Liu et al., 2022; Hu et al., 2020), the results of sensitivity analysis in Xiamen was VOC sensitive; the relatively low $PM_{2.5}$ concentrations in Xiamen showed limited influence on solar radiation through scattering and absorption, but promoted heterogeneous reactions producing radicals to a certain extent. UV and T had significant positive and negative non-linear correlations with PAN, respectively. When UV changed between 0 and 50 W m^{-2} and T changed between 15 and 35 W m^{-2}, the CIs barely increased. In addition, when RH was more than 40 %, the increase in RH was unfavourable for PAN production in both seasons. Some studies also found that high water vapour content could remove PAN and its precursors (Yan et al., 2018; Ma et al., 2020). Overall, the multiple-factor GAM

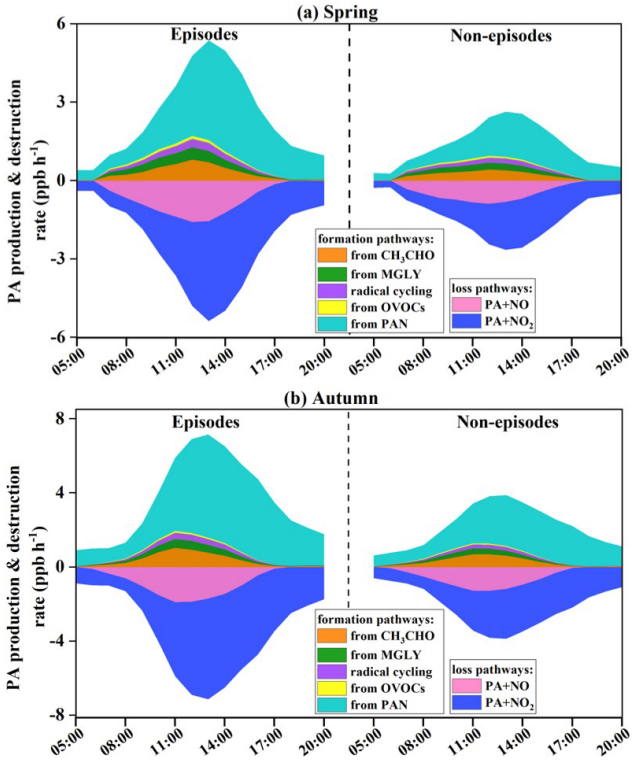

Figure 5. Formation and destruction rates of PA radical (hence PAN) during episodes and non-episodes in **(a)** spring and **(b)** autumn, respectively.

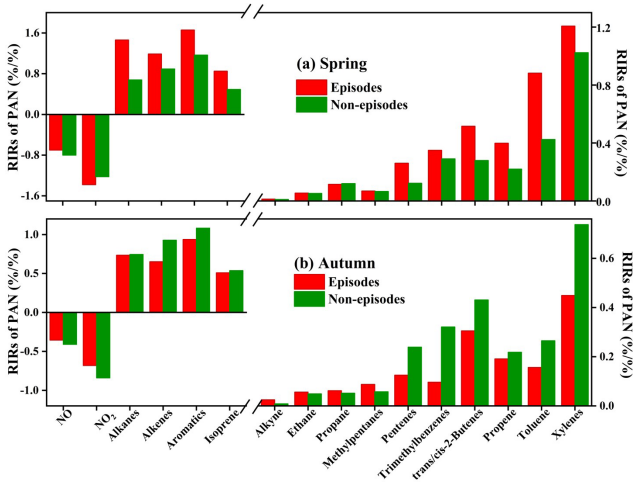

Figure 6. The OBM-MCM calculated relative incremental reactivity (RIR) for major PAN precursor groups and the top 10 specific species in **(a)** spring and **(b)** autumn during the day (06:00–17:00 local time).

analysis could better simulate the variations of PAN under real atmospheric conditions and evaluate the contributions of the influence factors to PAN formation.

3.3 Formation mechanism of PAN

3.3.1 Diurnal variation during episodes and non-episodes

Throughout the 53 d campaign, 30 and 21 d (i.e. 57 % and 40 %) with the peak values of PAN exceeding 2 ppbv were observed in spring and autumn, respectively. The scenarios of episodes and non-episodes were classified according to the previous method (Xue et al., 2014). Diurnal variations of air pollutants and meteorological parameters during episodes and non-episodes are shown in Fig. 4, which could be explained by the evolution of the planetary boundary layer, local emissions, and atmospheric photochemistry. PAN reached a maximum value at 12:00–14:00, then decreased with weak solar radiation and reached the lowest values in the early morning. Similar diurnal patterns of PAN and O_3 were observed, indicating the dominance of local photochemistry during the observation period (Zeng et al., 2019). CO, NO_x, and TVOCs showed the highest values in the morning and the lowest values in the afternoon.

In autumn, averaged PAN and O_3 during episodes (PAN: 1.08 ± 0.87 ppbv, and O_3: 40.06 ± 20.27 ppbv) were higher than those during non-episodes (PAN: 0.74 ± 0.41 ppbv, and O_3: 35.36 ± 13.95 ppbv). Meanwhile, some air pollutants and meteorological parameters during episodes were 1.03–1.40 times higher than those during non-episodes. The rainfall in Xiamen is more frequent in spring (Hu et al., 2020), leading to the obvious differences in UV and RH levels between episodes and non-episodes. In spring, the precursors (CO, NO_x, TVOCs) of PAN during episodes were 1.04–1.49 times lower than those during non-episodes. Moreover, the PAN and O_3 mixing ratios during episodes (PAN: 1.20 ± 0.81 ppbv, and O_3: 32.92 ± 19.81 ppbv) were still significantly higher than those during non-episodes (PAN: 0.64 ± 0.43 ppbv, and O_3: 18.65 ± 13.16 ppbv), attributing to the favourable meteorological conditions of photochemical reactions (strong UV, high T, and low RH). These results further explained that UV, O_x, and T in spring and O_x, TVOCs, T, and $PM_{2.5}$ in autumn played important roles in the formation of PAN based on the GAM analysis.

3.3.2 Formation and loss of PA radical

The formation and sink pathways of PA radical were further explored under different pollution scenarios (Fig. 5). Both the PA (hence PAN) production and destruction rates during episodes were 1.80 times higher than those during non-episodes. Combined with the analysis of Sect. 3.3.1, PA production rates during the day (06:00–17:00 local time) in autumn were 1.58 times higher than those in spring, even though the precursor levels in autumn were much lower compared with those in spring. These results indicated that favourable meteorological conditions were the dominant fac-

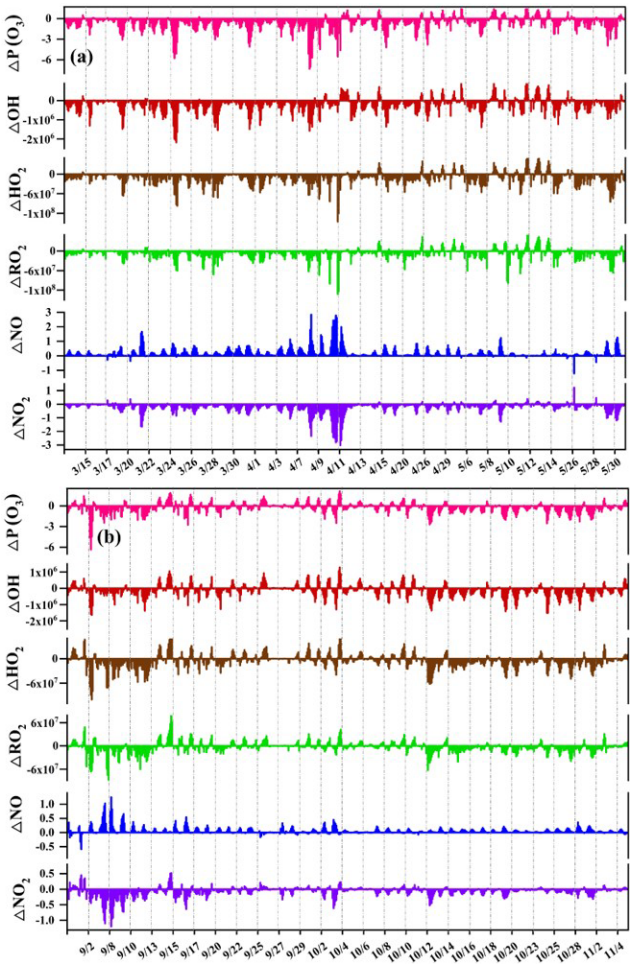

Figure 7. The differences of O_3 net production $\Delta P(O_3)$, ΔOH, ΔHO_2, ΔRO_2, ΔNO, and ΔNO_2 between the SC1 and the SC2 during the daytime (06:00–17:00) in **(a)** spring and **(b)** autumn (Unit: ppbv h^{-1} for $\Delta P(O_3)$; ppbv for ΔNO and ΔNO_2; molecules cm^{-3} for ΔOH, ΔHO_2, and ΔRO_2). The SC1 scenario was the base scenario putting all detected data (i.e. VOCs, trace gases, and meteorological parameters) into the model with all reaction pathways of the MCM mechanism, and the SC2 disabled the PAN chemistry, which is the only difference between SC1 and SC2.

tor to produce PAN through accelerating its production rate and accumulation. The thermal decomposition of PAN to PA radical in autumn accounted for $77\% \pm 12\%$ (episodes) and $73\% \pm 16\%$ (non-episodes) of total PA production, as well as $70\% \pm 12\%$ (episodes) and $64\% \pm 15\%$ (non-episodes) in spring, attributing to the relatively high air temperature and UV intensity. The thermal decomposition of PAN peaked at around 13:00–14:00 local time, when the air temperature was the highest in the day, and the pathways without considering the transform between PA and PAN peaked around noon (12:00 local time), when the solar radiation was the highest and photochemical reactions became the most intensive.

The average day PAN production rate from CH_3CHO by reacting with OH and NO_3 contributed 0.36 ± 0.25 ppb h^{-1} and 0.24 ± 0.13 ppb h^{-1} during episodes and non-episodes in spring. While the rate of 0.46 ± 0.35 ppb h^{-1} and 0.34 ± 0.24 ppb h^{-1} during episodes and non-episodes were observed in autumn. The second production reaction was photolysis and oxidation by OH and NO_3 of MGLY (episodes: 0.25 ± 0.15 ppb h^{-1} and non-episodes: 0.17 ± 0.08 ppb h^{-1} in spring; episodes: 0.24 ± 0.17 ppb h^{-1} and non-episodes: 0.16 ± 0.11 ppb h^{-1} in autumn). Then, the processes of radical cycling, including RO radical decomposition and reactions of acyl peroxy radicals with NO, were also the important sources to produce PA, with the contributions of $20\% \pm 3\%$ and $18\% \pm 3\%$ in spring and autumn, respectively. PA from the other OVOCs (not including CH_3CHO, MGLY, MVK, MACR, and acetone) through reactions of photolysis and oxidation by OH, NO_3, and O_3, accounted for $7\% \pm 2\%$ and $6\% \pm 1\%$ in spring and autumn, respectively. Other reactions of acetone, MVK, MACR, MPAN, and isoprene had a minor contribution (around 1 % in total) to PA formation. In contrast, the major contributor of PAN destruction rate was $PA + NO_2$ ($69\% \pm 16\%$ in spring and $73\% \pm 14\%$ in autumn), followed by $PA + NO$ ($31\% \pm 17\%$ and $27\% \pm 13\%$), while the other reactions with NO_3, HO_2, and RO_2 contributed limitedly (around 0.1 % of the total).

The second-generation precursors of PAN of CH_3CHO and MGLY have both primary and secondary sources, and the other OVOCs are mainly oxidation products of hydrocarbons (Pallavi, Sinha and Sinha, 2019; Sarkar et al., 2017). Consequently, the contribution and importance of first-generation precursors of PAN are necessary to identify to better control photochemical pollution, which will be discussed in the next section.

3.3.3 Sensitivity of PAN precursors

The OBM-MCM model analysis could be used to examine the relationship between PAN and its precursors, and quantify the contribution of first-generation precursors (Liu et al., 2021; Cardelino and Chameides, 1995). During these simulations (except for NO and NO_2), the model was not constrained by the OVOC measurements considering that these first-generation precursors contribute to PAN production through formation of OVOCs. The relative incremental reactivities (RIRs) for O_3 and PAN are shown in Fig. 6 and Fig. S7 in the Supplement. The PAN production was highly VOC sensitive, while the RIRs of NO and NO_2 were negative ranging from -0.17 to -1.94 during the day (06:00–17:00 local time). The result was consistent with the actual situation that vehicle exhausts were very important pollution sources in Xiamen. The ratio of $VOCs/NO_x$ (1.11 ± 0.32) also convinced us that NO_x was not the limiting factor on the photochemical reaction (Tan et al., 2019). In suburban or rural areas, the transition regime and NO_x-sensitive for PAN and O_3 production were usually found (Xue et al., 2014; Liu

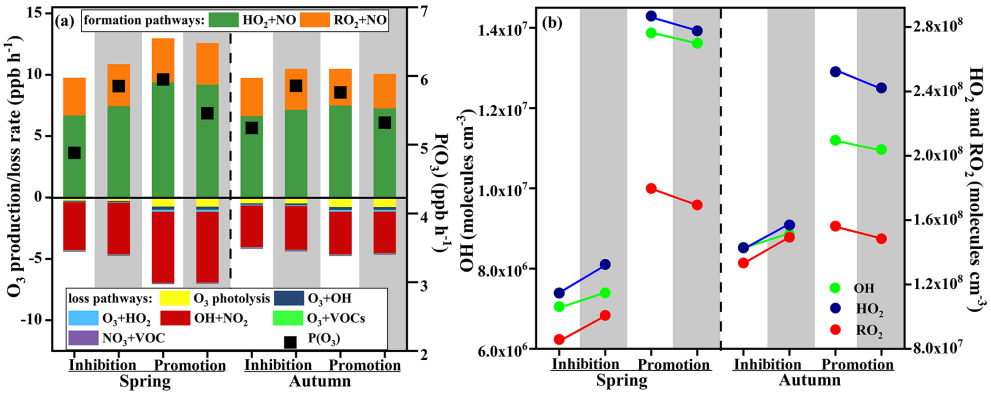

Figure 8. Model-simulated **(a)** net O_3 production rate and O_3 budgets, **(b)** OH, HO_2, and RO_2 on the inhibition effect stages and promotion effect stages. Note: the white background parts represent the SC1 scenarios using the MCM mechanism, and the grey background parts represent the SC2 scenarios using the MCM mechanism with PAN chemistry disabled.

et al., 2021). Zeng et al. (2019) found NO_2-positive and NO-negative to PAN formation in a suburban area of Hong Kong, consistent with the fact that NO_2 directly produced PAN and NO consumed PA radical inhibiting PAN formation.

As shown in Fig. 6, aromatics showed the largest RIRs for PAN in spring (1.41) and autumn (1.03), followed by alkanes (1.04 in spring and 0.78 in autumn), alkenes (1.04 and 0.74), and isoprene (0.67 and 0.52). The sensitivities of PAN precursors in spring were 1.37–2.07 times higher than those in autumn, due to the large percentages of PAN decomposition at high air temperatures in autumn. In spring, the weak solar radiation led to poor photochemical reactions, so the RIRs of PAN during non-episodes were lower than that during episodes. However, the PAN sensitivities during episodes were lower than those during non-episodes, attributed to the rapid PAN decomposition in autumn (Liu et al., 2021). In addition, RIRs of VOCs and NO_x for PAN were significantly higher than those of O_3 (Fig. S5 in the Supplement). For RIRs of VOCs, except for air temperature, the different formation mechanisms of PAN and O_3 should be considered. Only a small part of the VOCs could produce PA to form PAN; therefore, the VOCs were insufficient to produce PAN (Fischer et al., 2014). For RIRs of NO_x, O_3 was produced from the NO_2 conversion process, and was also rapidly consumed by NO titration. High levels of VOCs and NO_x enhanced the PAN formation, even though a pathway of NO destructed PAN, which was negligible compared with thermal decomposition. For this reason, the RIRs of NO_x for PAN were higher than those for O_3.

In addition, the top 10 VOCs species (including xylenes, toluene trans/cis-2-butenes, trimethylbenzenes, propene, pentenes, and methypentanes) governing PAN production were further identified (Fig. 6). The results suggested that the reduction of aromatics, alkenes, and alkanes with ≤ 5 carbons could effectively decrease PAN pollution.

3.4 Impacts of PAN on O_3 formation

3.4.1 Inhibition and promotion effect of PAN on O_3 formation

PAN could affect O_3 production by acting as a temporary source of NO_x or sink of PA radical to affect precursors and radical chemistry in the troposphere (Xia et al., 2021). To quantify the changes of O_3 in response to PAN chemistry in the coastal city, two parallel scenarios (SC1 and SC2) were conducted based on the OBM model. The SC1 was the base scenario putting all detected data (i.e. VOCs, trace gases, and meteorological parameters) into the model with all reaction pathways (as described in Sect. 2.2), and the SC2 disabled the PAN chemistry, which is the only difference between SC2 and SC1. Figure 7 shows the differences of O_3 net production rates $P(O_3)$, OH, HO_2, RO_2, NO, and NO_2 between the SC1 and the SC2. Negative and positive values represented the inhibition and promotion effects of PAN photochemistry on O_3 formation, respectively. Overall, PAN mostly inhibited the O_3 formation during the observation days. $P(O_3)$ had significantly positive correlations with OH ($R^2 = 0.96$ in spring and 0.95 in autumn), HO_2 ($R^2 = 0.91$ and 0.96), RO_2 ($R^2 = 0.86$ and 0.86), and NO_2 ($R^2 = 0.72$ and 0.85), and negative correlation with NO ($R^2 = -0.63$ and -0.65). As shown in Fig. S8 in the Supplement, the promotion effects of PAN on O_3 mainly happened during the periods of 11:00–16:00 local time, and most of them concentrated on PAN pollution episodes. The percentage of negative $P(O_3)$ values were 83 % and 69 % in spring and autumn, defined as "inhibition effect stages", while the positive $P(O_3)$ values accounted for 17 % and 31 % in spring and autumn, defined as "promotion effect stages".

Figure 8 shows the variations of modelled $P(O_3)$, O_3 budgets, and RO_x on the inhibition and promotion effect stages in spring and autumn. The abundance of RO_x in autumn (2.85×10^8 molecules cm^{-3}) was higher than that in spring (2.08×10^8 molecules cm^{-3}) during inhibition effect stages,

Table 2. Estimated degree (during promotion effect scenarios in spring and autumn) of freedom (Edf), degree of reference (Ref.df), P value, F value, deviance explained (%), adjusted R^2, and deviance contribution (%) for the smoothed variables (including NO, RO_x, TVOCs, $PM_{2.5}$, UV, T, RH, and WS) in the multiple-factor GAM model.

Smoothed variables	Incipient				Adjusted			
	Edf	Ref.df	F value	P value	Edf	Ref.df	F value	P value
Promotion effect stages in spring								
NO (ppbv)	5.58	6.39	2.09	0.06	Deleted			
RO_x (molecules cm^{-3})	5.99	7.06	22.88	0.00	5.72	6.83	21.56	0.00
TVOCs (ppbv)	1.14	1.26	0.60	0.40	Deleted			
$PM_{2.5}$ (ppbv)	1.98	2.51	2.62	0.07	Deleted			
UV ($W\,m^{-2}$)	3.89	4.80	7.40	0.00	2.98	3.73	9.66	0.00
T (°)	1.00	1.00	1.88	0.17	Deleted			
RH (%)	1.00	1.00	0.86	0.36	Deleted			
WS ($m\,s^{-1}$)	1.41	1.71	3.03	0.13	Deleted			
Promotion effect stages in autumn								
NO (ppbv)	1.15	1.28	0.20	0.66	Deleted			
RO_x (molecules cm^{-3})	7.10	8.06	41.04	0.00	7.37	8.26	45.45	0.00
TVOCs (ppbv)	1.00	1.00	0.00	0.97	Deleted			
$PM_{2.5}$ ($\mu g\,m^{-3}$)	1.00	1.00	0.53	0.47	Deleted			
UV ($W\,m^{-2}$)	3.11	3.87	28.90	0.00	3.07	3.83	30.55	0.00
T (°)	2.26	2.87	4.73	0.01	2.28	2.88	7.41	0.00
RH (%)	1.50	1.87	0.58	0.62	Deleted			
WS ($m\,s^{-1}$)	4.67	5.76	2.73	0.02	4.53	5.60	3.66	0.00

while the $P(O_3)$ value in autumn (5.24 ppbv h^{-1}) was higher than that in spring (4.88 ppbv h^{-1}). On the contrary, the level of RO_x in spring (4.81×10^8 molecules cm^{-3}) was higher than that in autumn (4.20×10^8 molecules cm^{-3}) during promotion effect stages, and the $P(O_3)$ value (5.95 ppbv h^{-1}) in spring was higher than that in autumn (5.76 ppbv h^{-1}). The results indicated that high RO_x concentration was an important factor for the formation of O_3. In the case of closing PAN photochemistry, the $P(O_3)$ increased 1.20 and 1.12 times during inhibition effect stages and decreased 1.09 and 1.08 times during promotion effect stages in spring and autumn, respectively (Fig. 8a). This was consistent with the corresponding changes in RO_x radical (Fig. 8b). During the inhibition effect stages, the averaged concentrations of OH, HO_2, and RO_2 increased 1.05, 1.16, and 1.17 times in spring, and increased 1.04, 1.10, and 1.12 times in autumn. During the promotion effect stages, the averaged concentrations of OH, HO_2, and RO_2 decreased 1.02, 1.03, and 1.06 times in spring, and decreased 1.02, 1.04, and 1.05 times in autumn. These results indicated that the changes in RO_x dominated the $P(O_3)$ trend without PAN photochemistry. Furthermore, the $P(O_3)$ level during promotion effect stages (5.95 ppbv h^{-1} in spring, 5.76 ppbv h^{-1} in autumn) was higher than that during inhibition effect stages (4.88 ppbv h^{-1} in spring, 5.24 ppbv h^{-1} in autumn). For model-simulated $P(O_3)$ and O_3 budgets (Fig. 8a), $HO_2 + NO$ (account for $70\% \pm 4\%$) and $RO_2 + NO$ ($30\% \pm 6\%$) were the main pathways of O_3 formation, and the main loss reactions were $OH + NO_2$ ($83\% \pm 12\%$).

PAN competed with O_3 precursors and terminated the radical chain to suppress O_3 formation by decreasing the RO_x production during the inhibition effect stages. During the promotion effect stages, the intensive atmospheric oxidation capacity and photochemical reaction enhance the RO_x formation rates from PAN to promote O_3 formation (Fig. 8b).

3.4.2 The influencing factors during inhibition and promotion stages

Table S4 in the Supplement shows the air pollutants and meteorological parameters during the inhibition effect stages and promotion effect stages. In detail, the levels of CO and the precursors of O_3 and PAN during the inhibition effect stages were significantly higher than those during the promotion effect stages. However, the $PM_{2.5}$ level during the inhibition effect stages was relatively lower than that during the promotion effect stages, reflecting the influence of heterogeneous reactions on $PM_{2.5}$ by supplying key photochemical oxidants to enhance PAN production (Xu et al., 2021). In addition, SO_2 and wind speed were comparable during the two scenarios. During the promotion effect stages, UV and T were significantly high, while P and RH were significantly low ($P < 0.01$). Meanwhile, the PAN (1.89 in spring, 1.58 ppbv in autumn) and O_3 (50.26 ppbv in spring and 53.51

in autumn) under the promotion effects were higher than those under the inhibition effects (PAN: 1.04 and 0.84 ppbv; O_3: 27.32 and 36.42 ppbv in spring and autumn, respectively).

In general, RO_x radicals dominated the atmospheric oxidative capacity and were the indicators of atmospheric photochemical reaction (Li et al., 2018). According to Sect. 3.2 of the GAM analysis, we chose the factors of NO, TVOCs, $PM_{2.5}$, UV, T, RH, WS, and RO_x ($RO_x = OH + HO_2 + RO_2$), to discuss the key influencing factors under promotion effect stages. Here, the $P(O_3)$ rate and the relevant influencing factors were set as the response and explanatory variables, respectively. Table 2 shows the influencing factors on $P(O_3)$ under promotion effects in spring and autumn. The factors that did not pass the significance test were deleted. As the adjusted model shows, the adjusted R^2 and deviance explained for the smoothed variables in four GAM models ranged from 0.67 to 0.78 and 70 % to 80 %, respectively, verifying the good fitting effect of the multiple-factor GAM model. According to the F values, the effects of RO_x (21.56 in spring; 45.45 in autumn) and UV (9.66 in spring; 30.55 in autumn) were the main factors leading to the promotion effect in both seasons. Both RO_x and UV had significant positive non-linear relationships with $P(O_3)$ during promotion effect stages in both seasons (Figs. S9 and S10 in the Supplement). The minor influences of WS and T were observed in autumn. The promotion effects easily happened during periods of favourable meteorological conditions for photochemical reactions.

Liu et al. (2021) found that PAN photochemistry inhibited O_3 production under low-NO_x and low-RO_x conditions, and promoted O_3 formation under high-NO_x conditions. However, in our study, surplus NO_x prevented NO_x from being the limiting factor photochemical formation of secondary pollution and the change in NO_x could be ignored. Whether PAN photochemistry suppressed or enhanced O_3 production mainly depended on the meteorological conditions of photochemical reaction and the RO_x levels.

4 Conclusions

Field observation was continuously conducted in spring and autumn in a coastal city of Southeast China. We clarified the seasonal variations of PAN pollution, formation mechanisms, influencing factors, and impacts on O_3 production. The average levels of PAN in autumn were lower than those in spring, while the O_3 showed the opposite characteristics. The multiple-factor GAM model showed that the key factors on the PAN mixing ratio were UV, O_x, and T in spring, while O_x, TVOCs, T, and $PM_{2.5}$ played important roles in PAN formation in autumn. The MCM model is an ideal tool to explore PAN photochemical formation and its key precursors at the species level and provides more relevant suggestions for reducing photochemical pollution. The controlling emissions of aromatics and alkenes with ≤ 5 carbons were beneficial for PAN pollution mitigation, and carbonyl compounds, especially acetaldehyde, were dominant in the PAN production mechanism. PAN presented the inhibition or promotion effects on O_3 under different environmental conditions. The promotion effects of PAN on O_3 mainly happened during the periods of 11:00–16:00 local time, most of which concentrated on PAN pollution episodes. According to the GAM analysis, the levels of RO_x and UV were the main factors leading to the promotion effects in both seasons. Overall, PAN stimulated O_3 formation under high levels of UV, T, and RO_x in the coastal city. These results indicate that the monitoring of PAN and its precursors, and the quantification of its impacts on O_3 formation, have significant guidance on photochemical pollution control. The scientific analysis methods used in this study provide a reference for the research on the formation mechanism of PAN and O_3 in other regions.

Code and data availability. The observation data at this site are available from the authors upon request.

Supplement. The supplement related to this article is available online at: https://doi.org/10.5194/acp-22-4339-2022-supplement.

Author contributions. TL performed chemical modelling analyses of OBM-MCM and wrote the paper. TL collected the data and contributed to the data analysis. JC and YH designed and revised the paper. JC supported funding of observation and research. GC, LX, ML, YC, XJ, CY, and YC contributed to discussions of results. WH, QH, and HW provided part of the data in Xiamen.

Competing interests. The contact author has declared that neither they nor their co-authors have any competing interests.

Disclaimer. Publisher's note: Copernicus Publications remains neutral with regard to jurisdictional claims in published maps and institutional affiliations.

Acknowledgements. This study was funded by the Cultivating Project of Strategic Priority Research Program of the Chinese Academy of Sciences (XDPB1903), the FJIRSM&IUE Joint Research Fund (RHZX-2019-006), the Center for Excellence in Regional Atmospheric Environment, CAS (E0L1B20201), the Xiamen Youth Innovation Fund Project (3502Z20206094), the foreign cooperation project of Fujian Province (2020I0038), and Xiamen Atmospheric Environment Observation and Research Station of Fujian Province.

Financial support. This research has been supported by the Cultivating Project of Strategic Priority Research Program of the Chinese Academy of Sciences (XDPB1903), the FJIRSM&IUE Joint Research Fund (RHZX-2019-006), the Center for Excellence in Regional Atmospheric Environment, CAS (E0L1B20201), the Xiamen Youth Innovation Fund Project (3502Z20206094), the foreign cooperation project of Fujian Province (2020I0038), and Xiamen Atmospheric Environment Observation and Research Station of Fujian Province.

Review statement. This paper was edited by Tanja Schuck and reviewed by two anonymous referees.

References

Atkinson, R., Baulch, D. L., Cox, R. A., Crowley, J. N., Hampson, R. F., Hynes, R. G., Jenkin, M. E., Rossi, M. J., Troe, J., and IUPAC Subcommittee: Evaluated kinetic and photochemical data for atmospheric chemistry: Volume II – gas phase reactions of organic species, Atmos. Chem. Phys., 6, 3625–4055, https://doi.org/10.5194/acp-6-3625-2006, 2006.

Cardelino, C. A. and Chameides, W. L.: An observation-based model for analyzing ozone precursor relationships in the urban atmosphere, J. Air Waste Manag. Assoc., 45, 161–180, 1995.

Chen, T., Xue, L., Zheng, P., Zhang, Y., Liu, Y., Sun, J., Han, G., Li, H., Zhang, X., Li, Y., Li, H., Dong, C., Xu, F., Zhang, Q., and Wang, W.: Volatile organic compounds and ozone air pollution in an oil production region in northern China, Atmos. Chem. Phys., 20, 7069–7086, https://doi.org/10.5194/acp-20-7069-2020, 2020.

Fischer, E. V., Jaffe, D. A., Reidmiller, D. R., and Jaegle, L.: Meteorological controls on observed peroxyacetyl nitrate at Mount Bachelor during the spring of 2008, J. Geophys. Res.-Atmos., 115, D03302, https://doi.org/10.1029/2009jd012776, 2010.

Fischer, E. V., Jacob, D. J., Yantosca, R. M., Sulprizio, M. P., Millet, D. B., Mao, J., Paulot, F., Singh, H. B., Roiger, A., Ries, L., Talbot, R. W., Dzepina, K., and Pandey Deolal, S.: Atmospheric peroxyacetyl nitrate (PAN): a global budget and source attribution, Atmos. Chem. Phys., 14, 2679–2698, https://doi.org/10.5194/acp-14-2679-2014, 2014.

Gaffney, J. S., Marley, N., Cunningham, M. M., and Doskey, P. V.: Measurements of peroxyacyl nitrates (PANS) in Mexico city: implications for megacity air quality impacts on regional scales, Atmos. Environ., 33, 5003–5012, 1999.

Grosjean, E., Grosjean, D., Woodhouse, L. F., and Yang, Y. J.: Peroxyacetyl nitrate and peroxypropionyl nitrate in Porto Alegre, Brazil, Atmos. Environ., 36, 2405–2419, 2002.

Guan, L., Liang, Y., Tian, Y., Yang, Z., Sun, Y., and Feng, Y.: Quantitatively analyzing effects of meteorology and $PM_{2.5}$ sources on low visual distance, Sci. Total Environ., 659, 764–772, 2019.

Han, J., Lee, M., Shang, X., Lee, G., and Emmons, L. K.: Decoupling peroxyacetyl nitrate from ozone in Chinese outflows observed at Gosan Climate Observatory, Atmos. Chem. Phys., 17, 10619–10631, https://doi.org/10.5194/acp-17-10619-2017, 2017.

He, X. and Lin, Z. S.: Interactive effects of the influencing factors on the changes of $PM_{2.5}$ concentration based on GAM model, Environ. Sci., 38, 22–32, 2017.

Hu, B., Liu, T., Hong, Y., Xu, L., Li, M., Wu, X., Wang, H., Chen, J., and Chen, J.: Characteristics of peroxyacetyl nitrate (PAN) in a coastal city of southeastern China: Photochemical mechanism and pollution process, Sci. Total Environ., 719, 137493, doi:10.1016/j.scitotenv.2020.137493, 2020.

Hua, J., Zhang, Y., de Foy, B., Shang, J., Schauer, J. J., Mei, X., Sulaymon, I. D., and Han, T.: Quantitative estimation of meteorological impacts and the COVID-19 lockdown reductions on NO_2 and $PM_{2.5}$ over the Beijing area using Generalized Additive Models (GAM), J. Environ. Manage., 291, 112676, https://doi.org/10.1016/j.jenvman.2021.112676, 2021.

Jenkin, M. E., Saunders, S. M., Wagner, V., and Pilling, M. J.: Protocol for the development of the Master Chemical Mechanism, MCM v3 (Part B): tropospheric degradation of aromatic volatile organic compounds, Atmos. Chem. Phys., 3, 181–193, https://doi.org/10.5194/acp-3-181-2003, 2003.

Kleindienst, T. E.: Recent developments in the chemistry and biology of peroxyacetyl nitrate, Res. Chem. Intermed., 20, 335–384, 1994.

Li, B., Ho, S. S. H., Gong, S., Ni, J., Li, H., Han, L., Yang, Y., Qi, Y., and Zhao, D.: Characterization of VOCs and their related atmospheric processes in a central Chinese city during severe ozone pollution periods, Atmos. Chem. Phys., 19, 617–638, https://doi.org/10.5194/acp-19-617-2019, 2019.

Li, Z., Xue, L., Yang, X., Zha, Q., Tham, Y. J., Yan, C., Louie, P. K. K., Luk, C. W. Y., Wang, T., and Wang, W.: Oxidizing capacity of the rural atmosphere in Hong Kong, Southern China, Sci. Total Environ., 612, 1114–1122, https://doi.org/10.1016/j.scitotenv.2017.08.310, 2018.

Liu, L., Wang, X., Chen, J., Xue, L., Wang, W., Wen, L., Li, D., and Chen, T.: Understanding unusually high levels of peroxyacetyl nitrate (PAN) in winter in Urban Jinan, China, J. Environ. Sci. (China), 71, 249–260, https://doi.org/10.1016/j.jes.2018.05.015, 2018.

Liu, T., Hong, Y., Li, M., Xu, L., Chen, J., Bian, Y., Yang, C., Dan, Y., Zhang, Y., Xue, L., Zhao, M., Huang, Z., and Wang, H.: Atmospheric oxidation capacity and ozone pollution mechanism in a coastal city of southeastern China: analysis of a typical photochemical episode by an observation-based model, Atmos. Chem. Phys., 22, 2173–2190, https://doi.org/10.5194/acp-22-2173-2022, 2022.

Liu, T., Hu, B., Xu, X., Hong, Y., Zhang, Y., Wu, X., Xu, L., Li, M., Chen, Y., Chen, X., and Chen, J.: Characteristics of $PM_{2.5}$-bound secondary organic aerosol tracers in a coastal city in Southeastern China: Seasonal patterns and pollution identification, Atmos. Environ., 237, 117710, https://doi.org/10.1016/j.atmosenv.2020.117710, 2020a.

Liu, T., Hu, B., Yang, Y., Li, M., Hong, Y., Xu, X., Xu, L., Chen, N., Chen, Y., Xiao, H., and Chen, J.: Characteristics and source apportionment of $PM_{2.5}$ on an island in Southeast China: Impact of sea-salt and monsoon, Atmos. Res., 235, 104786, https://doi.org/10.1016/j.atmosres.2019.104786, 2020b.

Liu, Y., Shen, H., Mu, J., Li, H., Chen, T., Yang, J., Jiang, Y., Zhu, Y., Meng, H., Dong, C., Wang, W., and Xue, L.: Formation of peroxyacetyl nitrate (PAN) and its impact on ozone production in the coastal atmosphere of

Qingdao, North China, Sci. Total Environ., 778, 146265, https://doi.org/10.1016/j.scitotenv.2021.146265, 2021.

Lonneman, W. A., Bufalini, J. J., and Seila, R. L.: PAN and oxidant measurement in ambient atmospheres, Environ. Sci. Technol., 10, 374–380, 1976.

Ma, Y., Ma, B., Jiao, H., Zhang, Y., Xin, J., and Yu, Z.: An analysis of the effects of weather and air pollution on tropospheric ozone using a generalized additive model in Western China: Lanzhou, Gansu, Atmos. Environ., 224, 117342, https://doi.org/10.1016/j.atmosenv.2020.117342, 2020.

Marley, N. A., Gaffney, J. S., Ramos-Villegas, R., and Cárdenas González, B.: Comparison of measurements of peroxyacyl nitrates and primary carbonaceous aerosol concentrations in Mexico City determined in 1997 and 2003, Atmos. Chem. Phys., 7, 2277–2285, https://doi.org/10.5194/acp-7-2277-2007, 2007.

Monks, P. S.: A review of the observations and origins of the spring ozone maximum, Atmos. Environ., 34, 3545–3561, 2000.

Moore, D. P. and Remedios, J. J.: Seasonality of Peroxyacetyl nitrate (PAN) in the upper troposphere and lower stratosphere using the MIPAS-E instrument, Atmos. Chem. Phys., 10, 6117–6128, https://doi.org/10.5194/acp-10-6117-2010, 2010.

Pallavi, Sinha, B., and Sinha, V.: Source apportionment of volatile organic compounds in the northwest Indo-Gangetic Plain using a positive matrix factorization model, Atmos. Chem. Phys., 19, 15467–15482, https://doi.org/10.5194/acp-19-15467-2019, 2019.

Penkett, S. A. and Brice, K. A.: The spring maximum in Photooxidants in the northern hemisphere troposphere, Nature, 319, 655–657, 1986.

Qian, X., Shen, H., and Chen, Z.: Characterizing summer and winter carbonyl compounds in Beijing atmosphere, Atmos. Environ., 214, 116845, https://doi.org/10.1016/j.atmosenv.2019.116845, 2019.

Roberts, J. M., Stroud, C. A., Jobson, B. T., Trainer, M., Hereid, D., Williams, E., Fehsenfeld, F., Brune, W., Martinez, M., and Harder, H.: Application of a sequential reaction model to PANs and aldehyde measurements in two urban areas, Geophys. Res. Lett., 28, 4583–4586, 2001.

Rubio, M. A., Lissi, E., Villena, G., Caroca, V., Gramsch, E., and Ruiz, A.: Estimation of hydroxyl and hydroperoxyl radicals concentrations in the urban atmosphere of Santiago, J. Chil. Chem. Soc., 50, 471–476, 2005.

Sarkar, C., Sinha, V., Sinha, B., Panday, A. K., Rupakheti, M., and Lawrence, M. G.: Source apportionment of NMVOCs in the Kathmandu Valley during the SusKat-ABC international field campaign using positive matrix factorization, Atmos. Chem. Phys., 17, 8129–8156, https://doi.org/10.5194/acp-17-8129-2017, 2017.

Saunders, S. M., Jenkin, M. E., Derwent, R. G., and Pilling, M. J.: Protocol for the development of the Master Chemical Mechanism, MCM v3 (Part A): tropospheric degradation of non-aromatic volatile organic compounds, Atmos. Chem. Phys., 3, 161–180, https://doi.org/10.5194/acp-3-161-2003, 2003.

Sun, M., Cui, J. N., Zhao, X. M., and Zhang, J. B.: Impacts of precursors on peroxyacetyl nitrate (PAN) and relative formation of PAN to ozone in a southwestern megacity of China, Atmos. Environ., 231, 117542, https://doi.org/10.1016/j.atmosenv.2020.117542, 2020.

Tan, Z., Lu, K., Jiang, M., Su, R., Wang, H., Lou, S., Fu, Q., Zhai, C., Tan, Q., Yue, D., Chen, D., Wang, Z., Xie, S., Zeng, L., and Zhang, Y.: Daytime atmospheric oxidation capacity in four Chinese megacities during the photochemically polluted season: a case study based on box model simulation, Atmos. Chem. Phys., 19, 3493–3513, https://doi.org/10.5194/acp-19-3493-2019, 2019.

Temple, P. J. and Taylor, O. C.: World-wide ambient measurements of peroxyacetyl nitrate (PAN) and implications for plant injury, Atmos. Environ., 17, 1583–1587, 1983.

Tyndall, G. S., Cox, R.A., Granier, C., Lesclaux, R., Moortgat, G. K., Pilling, M. J., Ravishankara, A. R., and Wallington, T. J.: Atmospheric chemistry of small organic peroxy radicals, J. Geophys. Res.-Atmos., 106, 12157–12182, 2001.

Wolfe, G. M., Cantrell, C., Kim, S., Mauldin III, R. L., Karl, T., Harley, P., Turnipseed, A., Zheng, W., Flocke, F., Apel, E. C., Hornbrook, R. S., Hall, S. R., Ullmann, K., Henry, S. B., DiGangi, J. P., Boyle, E. S., Kaser, L., Schnitzhofer, R., Hansel, A., Graus, M., Nakashima, Y., Kajii, Y., Guenther, A., and Keutsch, F. N.: Missing peroxy radical sources within a summertime ponderosa pine forest, Atmos. Chem. Phys., 14, 4715–4732, https://doi.org/10.5194/acp-14-4715-2014, 2014.

Wu, X., Xu, L., Hong, Y., Chen, J., Qiu, Y., Hu, B., Hong, Z., Zhang, Y., Liu, T., Chen, Y., Bian, Y., Zhao, G., Chen, J., and Li, M.: The air pollution governed by subtropical high in a coastal city in Southeast China: Formation processes and influencing mechanisms, Sci. Total Environ., 692, 1135–1145, https://doi.org/10.1016/j.scitotenv.2019.07.341, 2019.

Wu, X., Li, M., Chen, J., Wang, H., Xu, L., Hong, Y., Zhao, G., Hu, B., Zhang, Y., Dan, Y., and Yu, S.: The characteristics of air pollution induced by the quasi-stationary front: Formation processes and influencing factors, Sci. Total Environ., 707, 136194, https://doi.org/10.1016/j.scitotenv.2019.136194, 2020.

Xia, S. Y., Zhu, B., Wang, S. X., Huang, X. F., and He, L. Y.: Spatial distribution and source apportionment of peroxyacetyl nitrate (PAN) in a coastal region in southern China, Atmos. Environ., 260, 118553, https://doi.org/10.1016/j.atmosenv.2021.118553, 2021.

Xu, W., Zhang, G., Wang, Y., Tong, S., Zhang, W., Ma, Z., Lin, W., Kuang, Y., Yin, L., and Xu, X.: Aerosol Promotes Peroxyacetyl Nitrate Formation During Winter in the North China Plain, Environ. Sci. Technol., 55, 3568–3581, https://doi.org/10.1021/acs.est.0c08157, 2021.

Xu, X., Zhang, H., Lin, W., Wang, Y., Xu, W., and Jia, S.: First simultaneous measurements of peroxyacetyl nitrate (PAN) and ozone at Nam Co in the central Tibetan Plateau: impacts from the PBL evolution and transport processes, Atmos. Chem. Phys., 18, 5199–5217, https://doi.org/10.5194/acp-18-5199-2018, 2018.

Xue, L., Wang, T., Wang, X., Blake, D. R., Gao, J., Nie, W., Gao, R., Gao, X., Xu, Z., Ding, A., Huang, Y., Lee, S., Chen, Y., Wang, S., Chai, F., Zhang, Q., and Wang, W.: On the use of an explicit chemical mechanism to dissect peroxy acetyl nitrate formation, Environ. Pollut., 195, 39–47, 2014.

Xue, L., Gu, R., Wang, T., Wang, X., Saunders, S., Blake, D., Louie, P. K. K., Luk, C. W. Y., Simpson, I., Xu, Z., Wang, Z., Gao, Y., Lee, S., Mellouki, A., and Wang, W.: Oxidative capacity and radical chemistry in the polluted atmosphere of Hong Kong and Pearl River Delta region: analysis of a severe photo-

chemical smog episode, Atmos. Chem. Phys., 16, 9891–9903, https://doi.org/10.5194/acp-16-9891-2016, 2016.

Yan, R. E., Ye, H., Lin, X., He, X., Chen, C., Shen, J. D., Xu, K. E., Zhen, X. Y., and Wang, L. J.: Characteristics and influence factors of ozone pollution in Hangzhou, Acta Sci. Circumstantiae, 38, 1128–1136, 2018.

Yuan, J., Ling, Z., Wang, Z., Lu, X., Fan, S., He, Z., Guo, H., Wang, X., and Wang, N.: PAN–Precursor Relationship and Process Analysis of PAN Variations in the Pearl River Delta Region, Atmosphere, 9, 372, https://doi.org/10.3390/atmos9100372, 2018.

Zeng, L. W., Fan, G. J., Lyu, X. P., Guo, H., Wang, J. L., and Yao, D. W.: Atmospheric fate of peroxyacetyl nitrate in suburban Hong Kong and its impact on local ozone pollution, Environ. Pollut., 252, 1910–1919, 2019.

Zhang, B. Y., Zhao, X. M., and Zhang, J. B.: Characteristics of peroxyacetyl nitrate pollution during a 2015 winter haze episode in Beijing, Environ. Pollut., 244, 379–387, 2019.

Zhang, G., Mu, Y. J., Zhou, L. X., Zhang, C. L., Zhang, Y. Y., Liu, J. F., Fang, S. X., and Yao, B.: Summertime distributions of peroxyacetyl nitrate (PAN) and peroxypropionyl nitrate (PPN) in Beijing: understanding the sources and major sink of PAN, Atmos. Environ., 103, 289–296, 2015.